



1           **Numerical modeling on the mechanisms of chlorine**  
2           **chemistry in snowpack and their impact on secondary**  
3           **atmospheric pollution**

4  
5   Shengjin Xie<sup>1,3</sup>, Xuelei Zhang<sup>1,2</sup>, Aijun Xiu<sup>1</sup>, Hong Qi<sup>3</sup>, Shengrui Tong<sup>4</sup>, Qianjie Chen<sup>5</sup>, Chao Gao<sup>1</sup>,  
6   Hongmei Zhao<sup>1</sup>, Shichun Zhang<sup>1</sup>, Stephen Dauda Yabo<sup>6</sup>, Yiming Liu<sup>7</sup>, and Siting Li<sup>7</sup>, Mengduo  
7   Zhang<sup>8</sup>

8   <sup>1</sup> State Key Laboratory of Black Soils Conservation and Utilization, Northeast Institute of  
9   Geography and Agroecology, Chinese Academy of Sciences, Changchun, China

10   <sup>2</sup> School of Geographical Sciences, Liaoning Normal University, Dalian, China

11   <sup>3</sup> School of Environment, Harbin Institute of Technology, Harbin, China

12   <sup>4</sup> State Key Laboratory for Structural Chemistry of Unstable and Stable Species, CAS  
13   Research/Education Center for Excellence in Molecular Sciences, Institute of Chemistry, Chinese  
14   Academy of Sciences, Beijing, China

15   <sup>5</sup> Department of Civil and Environmental Engineering, The Hong Kong Polytechnic University,  
16   Hong Kong SAR, China

17   <sup>6</sup> Department of Geomatics, Faculty of Environmental Design, Ahmadu Bello University, Zaria,  
18   Nigeria

19   <sup>7</sup> Guangdong Province Key Laboratory for Climate Change and Natural Disaster Studies, School of  
20   Atmospheric Sciences, Sun Yat-sen University, Guangzhou, China

21   <sup>8</sup> School of Urban and Rural Planning, Henan University of Economics and Law, Zhengzhou, China

22  
23   **Correspondence:** Xuelei Zhang ([zhangxuelei@iga.ac.cn](mailto:zhangxuelei@iga.ac.cn))

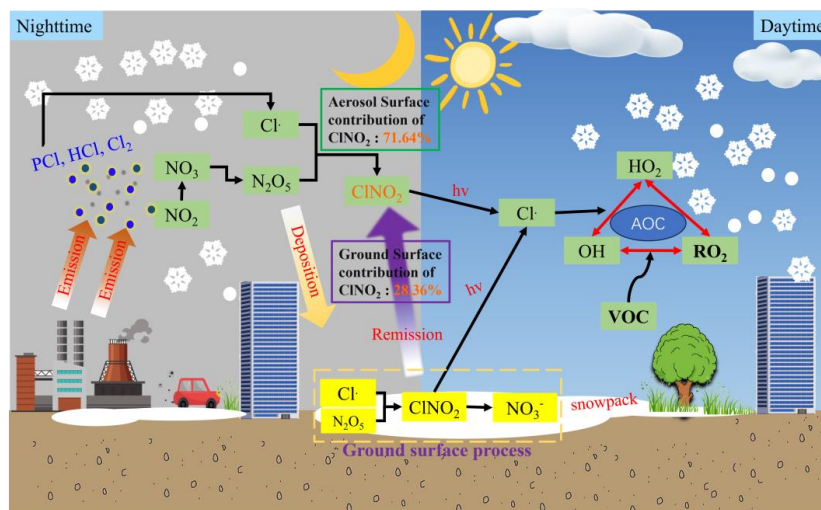
24   **Abstract**

25       Snow with high albedo enhances atmospheric photochemical reactions,  
26   influencing key oxidative processes. Nitryl chloride (ClNO<sub>2</sub>), as a strong oxidizing  
27   species, is generated by the heterogeneous reaction between dinitrogen pentoxide  
28   (N<sub>2</sub>O<sub>5</sub>) and chloride adsorbed on aerosol and the ground surfaces. After sunrise, the  
29   photolysis of ClNO<sub>2</sub> rapidly releases highly reactive chlorine radicals (Cl·), which  
30   contributes to the formation of secondary pollutants. However, the pollution  
31   mechanisms in high-latitude, snow-covered regions associated with increased chlorine  
32   emissions remain unclear. In this study, we employed the WRF-CAMx model (Weather  
33   Research and Forecasting Model-Comprehensive Air Quality Model with extensions)  
34   with a modified chemical mechanism (CB6r2h\_lts, Carbon Bond 6 revision 2 with  
35   heterogeneous chemistry for low-temperature and snow-covered conditions) that  
36   incorporated heterogeneous N<sub>2</sub>O<sub>5</sub> reactions and ClNO<sub>2</sub> photolysis on ground surfaces  
37   to assess their impact on regional atmosphere under snow-covered conditions in



38 Northeast China. Our findings reveal that under snow-covered conditions, the YU20  
 39 aerosol scheme (from study by YU et al., 2020) outperforms the BT09 scheme (from  
 40 study by Bertram et al., 2009) in simulating  $N_2O_5$  and  $ClNO_2$  concentrations within the  
 41 CAMx model. Incorporating anthropogenic chlorine emissions and ground surface  
 42 chemistry significantly improved model performance for  $ClNO_2$ , reducing the mean  
 43 bias (MB) from -105.78 pptv to 2.66 pptv and increasing the index of agreement (IOA)  
 44 from 0.39 to 0.86. These processes resulted in a maximum hourly increase of 3.65  
 45  $\mu\text{g}/\text{m}^3$  in  $PM_{2.5}$  (relative contribution: 15.34%) and 3.41 ppbv in MDA8  $O_3$  (5.68%).  
 46 Notably, ground surface chemical processes were identified as the dominant source of  
 47 nocturnal  $ClNO_2$ , contributing approximately 28.36% to nighttime accumulation across  
 48 Northeast China. These findings not only highlight the pivotal role of chlorine  
 49 chemistry in atmospheric processes under snow-covered conditions, but also provide  
 50 crucial support for the refinement of the mechanisms governing the flux exchange of  
 51 chemical substances between the atmosphere and the cryosphere.

52 Graphical abstract



53

54 **Keywords:** Snowpack; Numerical simulation; Reactive chlorine; Heterogeneous  
 55 chemistry; Ground surface process; CAMx model

56 1. Introduction

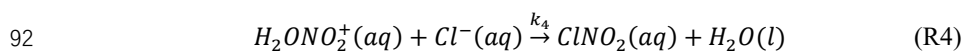
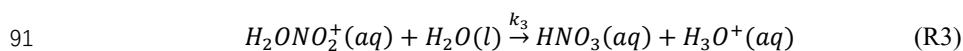
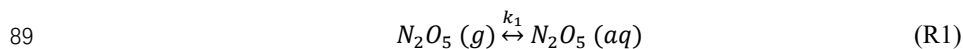
57 Reactive nitrogen and chlorine atoms are prominent active gases in the atmosphere,  
 58 influencing the budget of the atmospheric oxidizing capacity (AOC) (Yang et al., 2022).



59  $\text{N}_2\text{O}_5$  serves as a key species in nocturnal chemical reactions within the troposphere. It  
60 undergoes heterogeneous reactions with chlorine-containing aerosols and the surfaces  
61 of various media (vegetation, soil, snow, and buildings, etc.) to form nitryl chloride  
62 ( $\text{ClNO}_2$ ) (Wang et al., 2017; Wang et al., 2020; Jeong et al., 2023). Photolysis of  $\text{ClNO}_2$   
63 in the atmosphere produces highly reactive chlorine atoms (Cl) which react with  
64 alkanes at rates approximately two orders of magnitude faster than hydroxyl radicals  
65 (OH) (Jeong et al., 2023). Therefore, accurately quantifying the impact of  $\text{N}_2\text{O}_5$   
66 absorption coefficient ( $\gamma(\text{N}_2\text{O}_5)$ ) and  $\text{ClNO}_2$  yield ( $\phi(\text{ClNO}_2)$ ) at different interfaces is  
67 crucial for clarifying the contribution of  $\text{ClNO}_2$  to pollutants formation.

68 The  $\gamma(\text{N}_2\text{O}_5)$  represents the net probability of  $\text{N}_2\text{O}_5$  undergoing irreversible uptake  
69 by an aerosol surface upon collision. Accurately quantifying  $\gamma(\text{N}_2\text{O}_5)$  values under  
70 varying environmental conditions remains challenging, as this parameter demonstrably  
71 fluctuates in response to changes in nitrate concentration, liquid moisture content,  
72 chloride abundance, and organic matter content (Bertram and Thornton, 2009; Gaston  
73 et al., 2014; McDuffie et al., 2018; Mentel et al., 1999; Mielke et al., 2013; Tham et al.,  
74 2018; Thornton and Abbatt, 2005; Yu et al., 2020).

75 Prominent among existing parameterizations is that of Bertram and Thornton  
76 (2009), who proposed a method for calculating the uptake coefficient of  $\text{N}_2\text{O}_5$  on  
77 particulate matter surfaces (R1-R4) and the production yield of  $\text{ClNO}_2$  ( $\phi(\text{ClNO}_2)$ ) from  
78 environmental chamber experiments. This framework has been implemented in  
79 numerous regional air quality models (Dai et al., 2020; Li et al., 2016; Yu et al., 2020).  
80 However, field-based determinations consistently yield lower values than laboratory-  
81 derived estimates. Yu et al. (2020) synthesized observational data from multiple regions  
82 across China to refine  $\gamma(\text{N}_2\text{O}_5)$  estimates, demonstrating that laboratory-based  
83 parameterizations systematically overestimate this coefficient when compared against  
84 ambient measurements. Subsequent field investigations have corroborated that  
85 suppression of  $\gamma(\text{N}_2\text{O}_5)$  in North China is attributable to factors including reduced  
86 aerosol liquid water content (ALWC), elevated particulate nitrate ( $\text{pNO}_3$ ), and particle  
87 morphological characteristics (Wang et al., 2020), providing mechanistic insight into  
88 the observed discrepancies between simulated and measured values.



93 However, compared to aerosols, research on the heterogeneous hydrolysis process  
94 of  $N_2O_5$  on snowpack remains limited (George et al., 1994; Hanson and Ravishankara,  
95 1991; Lopez-Hilfiker et al., 2012; McNamara et al., 2021). Field observations have  
96 confirmed that ice and snow surfaces in the nighttime boundary layer of high-latitude  
97 cold regions catalyze the heterogeneous hydrolysis of  $N_2O_5$ , leading to  $ClNO_2$   
98 production (Apodaca et al., 2008; Huff et al., 2011; Wang et al., 2020). An upward net  
99 flux of  $ClNO_2$  was observed in near-surface snowpack regions, suggesting that saline  
100 snowpack may be a source of  $ClNO_2$  (McNamara et al., 2021).

101 From the perspective of snowpack modeling, accurately quantifying the  $N_2O_5$   
102 adsorption coefficient and the  $\phi(ClNO_2)$  on the snowpack, and coupling them into a  
103 one-dimensional numerical model, can provide valuable insights into the contribution  
104 of surface snow to this process (McNamara et al., 2020; Wang et al., 2020; Kulju et al.,  
105 2021; Jeong et al., 2023). In urban areas, winter snowpack can contribute up to 60% of  
106 near-surface  $ClNO_2$ , according to one-dimensional numerical models (Jeong et al.,  
107 2023). However, one-dimensional models have limitations in representing the  
108 complexity of air-snow exchanges. In contrast, our use of a three-dimensional air  
109 quality model, combined with dynamic calculations of surface chemical processes,  
110 allows for a more accurate representation of the crucial bidirectional flux exchange  
111 between the atmosphere and snow cover.

112 Northeast China experiences a protracted period of winter snow cover, with the  
113 heating season extending up to half a year. Large-scale coal burning has significantly  
114 increased chlorine emissions in the atmosphere (Liu et al., 2018; Li et al., 2024). These  
115 chlorides adsorb onto particulate matter surfaces, some of which are deposited onto  
116 snow, where they undergo heterogeneous reactions with  $N_2O_5$  to produce  $ClNO_2$

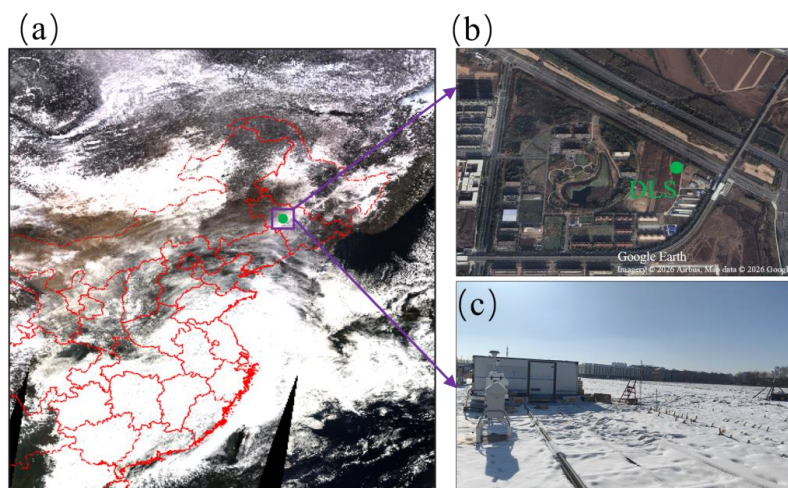


117 (McNamara et al., 2019; Wang et al., 2019; Jeong et al., 2023). These conditions  
118 establish the region as an ideal setting for investigating chlorine chemistry fluxes and  
119 for performing numerical simulations of air-snow interactions. In this study, we  
120 modified the WRF-CAMx model to include a parameterization for  $N_2O_5$  hydrolysis on  
121 aerosols and a coupled (3D) surface chemistry module to analyze the impacts on  
122 regional particulate matter and ozone formations under snow-cover condition in  
123 Northeast China.

## 124 2. Methodology

### 125 2.1 Field Observations

126 Field observations of  $N_2O_5$ ,  $ClNO_2$  and many other chemical species were  
127 conducted at the monitoring station of Northeast Institute of Geography and  
128 Agroecology (NIGA), Chinese Academy of Sciences from February 23 to March 3,  
129 2024 in Northeast China. The DLS site is in the experimental farmland in the northern  
130 suburbs of Changchun City (Fig. 1), with coordinates (44.0°N, 125.4°E). During the  
131 observation period, the campaign was characterized by recurrent snowfall events that  
132 maintained a continuous snow cover at the surface.  $N_2O_5$  and  $ClNO_2$  were measured  
133 using an iodide-adduct chemical ionization mass spectrometer (CIMS).



134  
135 **Figure 1** Sampling site (DLS) information: (a) Satellite-derived snow cover image  
136 (data source: National Snow and Ice Data Center, <https://nsidc.org/data>). (b) Traffic



137 conditions around the sampling site at the Northeast Institute of Geography and  
138 Agroecology, Chinese Academy of Sciences (NIGA), Jilin Province, China (Imagery  
139 © 2026 Airbus, Map data © 2026 Google, <https://earth.google.com/>). (c) The  
140 observation station surrounded by snow-covered farmland.

## 141 2.2 WRF-CAMx Model and Configuration

142 The CAMx v7.1 model, incorporating the newly developed low-temperature  
143 halogen chemical mechanism (CB6r2h\_lts), was employed to simulate the spatio-  
144 temporal distributions of atmospheric pollutants. The modeling domain was configured  
145 to cover the whole Northeast region of China, consisting of  $76 \times 78$  grid cells with a  
146 horizontal resolution of  $27 \text{ km} \times 27 \text{ km}$  and 29 vertical layers. The model simulation  
147 period with a 13-day spin-up was set from February 10th to March 2nd, 2024. Boundary  
148 and initial conditions were derived from the Whole Atmosphere Community Climate  
149 Model (WACCM, <https://www2.acom.ucar.edu/gcm/waccm>). Two anthropogenic  
150 emission inventories were employed: the Multi-resolution Emission Inventory for  
151 China (MEIC; <http://meicmodel.org.cn/>), which was processed to represent the  
152 Northeastern China region, and the Emissions Database for Global Atmospheric  
153 Research (EDGAR; <https://edgar.jrc.ec.europa.eu/>), used for areas outside China. The  
154 anthropogenic chlorine emissions inventory (ACEI) compiled by Sun Yat-sen  
155 university was adopted. Meteorological input data for the CAMx model were obtained  
156 from WRFV3.7.1, which utilizes a data nudging method ( $\text{guv, gt, gq} = 0.0001 \text{ s}^{-1}$ ). More  
157 detailed configuration of WRF-CAMx is listed in Table S1.

## 158 2.3 Localization of $\text{N}_2\text{O}_5$ adsorption reaction coefficients and $\text{ClNO}_2$ 159 production on aerosol surfaces

160 The  $\gamma(\text{N}_2\text{O}_5)$  is influenced by the  $\text{pNO}_3$ , organic matter,  $\text{Cl}^-$ , and aerosol liquid  
161 water content (ALWC) (R5-R7). Currently, the heterogeneous reaction parameters of  
162  $\text{N}_2\text{O}_5$  on aerosols in most air quality models (such as CAMx, CMAQ, etc.) are based  
163 on laboratory experiments (Bertram and Thornton, 2009). However, based on field  
164 observations, Yu et al. (2020) directly measured  $\gamma\text{N}_2\text{O}_5$  in ambient aerosols from two  
165 rural areas in northern China and Nanjing using an in-situ aerosol flow tube system.



166 The parameters of aerosol surfaces in the above two studies (BT09 and YU20) are  
167 shown in Table S2.

$$168 \quad \gamma(\text{N}_2\text{O}_5) = \frac{4 V_a}{c S_a} K_H k'_{2f} \left( 1 - \frac{1}{\left( \frac{k_3[\text{H}_2\text{O}(l)]}{k_2 b[\text{NO}_3^-]} \right) + 1 + \left( \frac{k_4[\text{H}_2\text{O}(l)]}{k_2 b[\text{Cl}^-]} \right)} \right) \quad (\text{R5})$$

$$169 \quad k'_{2f} = \beta - \beta e^{(-\delta[\text{H}_2\text{O}])} \quad (\text{R6})$$

$$170 \quad \phi(\text{ClNO}_2) = \left( 1 + \frac{k_3[\text{H}_2\text{O}(l)]}{k_4[\text{Cl}^-]} \right)^{-1} \quad (\text{R7})$$

171 Where  $V_a/S_a$  represents the volume-to-surface-area ratio of particles (units: m),  
172 serves as a key morphological parameter alongside  $K_H$ , the dimensionless Henry's law  
173 constant ( $K_H = [\text{N}_2\text{O}_5]_{\text{aq}}/[\text{N}_2\text{O}_5]_{\text{g}}$ ). To account for  $\text{H}_2\text{O}$  limitation in nitrate-free  
174 particles, the rate coefficient for  $R_{2f}$  is treated as a function of liquid water content and  
175 redefined as  $k'_{2f}$  in Eq. (R6). The yield of  $\text{ClNO}_2$ ,  $\phi(\text{ClNO}_2)$ , is given by Eq. (R7). The  
176 fitted constants  $k_3/k_{2b}$ ,  $k_4/k_{2b}$ ,  $k_3/k_4$  are showed (Table S2).

## 177 2.4 Coupling Heterogeneous Chemical Processes of $\text{N}_2\text{O}_5$ on the ground 178 Surface

179 The surface chemistry module is activated to simulate gas flux exchange between  
180 the atmosphere and the ground, accounting for the chemical reactions of  $\text{N}_2\text{O}_5$  on  
181 surfaces such as snow, vegetation, buildings and soil. However, the  $S/V_g$  parameter in  
182 the surface chemistry module is calculated as a one-dimensional plane, leading to an  
183 underestimation of the results of the model. To address this, we revised the surface  
184 chemistry module to dynamically calculate the  $S/V_g$  parameter based on 3D surfaces  
185 within each grid cell. To support this revision, we gathered data on surface area of  
186 buildings in Northeast China through field investigation and satellite retrieval. The  
187 detailed description of revising the surface chemistry module is shown in Fig. S1.

188  $\text{N}_2\text{O}_5$  deposited on snowpack surfaces undergoes simultaneous reactions with  
189 hydrochloric acid and water (Table 1), similar to the chemical reactions on aerosol  
190 surfaces. The calculation processes for  $\gamma(\text{N}_2\text{O}_5)$  and  $\phi(\text{ClNO}_2)$  on snow grains, which



191 depend on the temperature of the snow, are presented in Text S1. Under low-  
 192 temperature conditions,  $\phi(\text{ClNO}_2)$  is relatively high, reaching values over 0.80. At a  
 193 temperature close to approximately 273 K (0°C), both the  $\gamma(\text{N}_2\text{O}_5)$  and  $\phi(\text{ClNO}_2)$   
 194 showed a decreasing trend toward zero (Fig. S2).

195 **Table 1. Revised heterogeneous  $\text{N}_2\text{O}_5$  reactions in CAMx model.**

Interfaces	Reactions	Uptake coefficient ( $\gamma$ )	The yield of $\text{ClNO}_2$	Reaction rate constant ( $\text{s}^{-1}$ )	Reference
Aerosol	$\text{HCl} + \text{N}_2\text{O}_5$ $\xrightarrow{\text{Aerosol}} \text{ClNO}_2 + \text{HNO}_3$	(R5)	$\phi(\text{ClNO}_2)$ $= \left(1 + \frac{[\text{H}_2\text{O}(l)]}{103 * [\text{Cl}^-]}\right)^{-1}$	$k$ $= \frac{1}{4} \gamma_{\text{N}_2\text{O}_5} V_{\text{N}_2\text{O}_5} \frac{S}{V_g}$ $* \phi(\text{ClNO}_2)$	(Bertram and Thornton, 2009; Yu et al., 2020)
		220K $\leq$ T $\leq$ 258K: $\gamma_{\text{N}_2\text{O}_5} = 0.028$	220 K $\leq$ T $\leq$ 258 K: $\phi(\text{ClNO}_2) = 0.85$		
Ground	$\text{HCl} + \text{N}_2\text{O}_5$ $\xrightarrow{\text{Ground}} \text{ClNO}_2 + \text{HNO}_3$	259K $\leq$ T $\leq$ 272K: 272K: $\gamma_{\text{N}_2\text{O}_5} = 0.026$	259 K $\leq$ T $\leq$ 272 K: $\phi(\text{ClNO}_2) = 0.55$	$k$ $= \frac{1}{8} \gamma_{\text{N}_2\text{O}_5} V_{\text{N}_2\text{O}_5} \frac{S}{V_g}$ $* \phi(\text{ClNO}_2)$	(Jeong et al., 2023; Wang et al., 2020)
		T $\geq$ 273K: $\gamma_{\text{N}_2\text{O}_5} = 0.023$	T $\geq$ 273K: $\phi(\text{ClNO}_2) = 0.048$		
	$\text{ClNO}_2 + h\nu \xrightarrow{\text{Ground}} \text{Cl} + \text{NO}_2$	-	-	$J = 2.86 \times 10^{-4}$	(Jeong et al., 2023)

196 T represents the surface temperature; K is the reaction rate constant ( $\text{s}^{-1}$ ); J indicates the photolysis  
 197 rate constant ( $\text{s}^{-1}$ ).  $\phi$  ( $\text{ClNO}_2$ ) denotes the yield, without units.

## 199 2.5 Scenarios setting

200 This study investigates the impact of various aerosol schemes, ground chemistry  
 201 models, and anthropogenic chlorine emissions through six scenarios: B1, Y0, Y1, Y2,  
 202 Y3, and Y4 (Table 2).

203 Sensitivity analyses were conducted among different simulation scenarios, with  
 204 the specific configurations detailed as follows: Y3-Y0: The combined effects of  
 205 anthropogenic chlorine and heterogeneous chemistry of  $\text{N}_2\text{O}_5$ ; Y2-Y0: The impact of  
 206 anthropogenic chlorine emissions; Y2-Y1: The contribution of  $\text{N}_2\text{O}_5$  heterogeneous  
 207 chemistry on aerosol surfaces; Y3-Y2: The sensitivity analysis of ground surfaces  
 208 chemical processes; Y4-Y3: The contribution of  $\text{ClNO}_2$  surface photolysis.

209

210



211

Table 2. Scenario Design Schemes

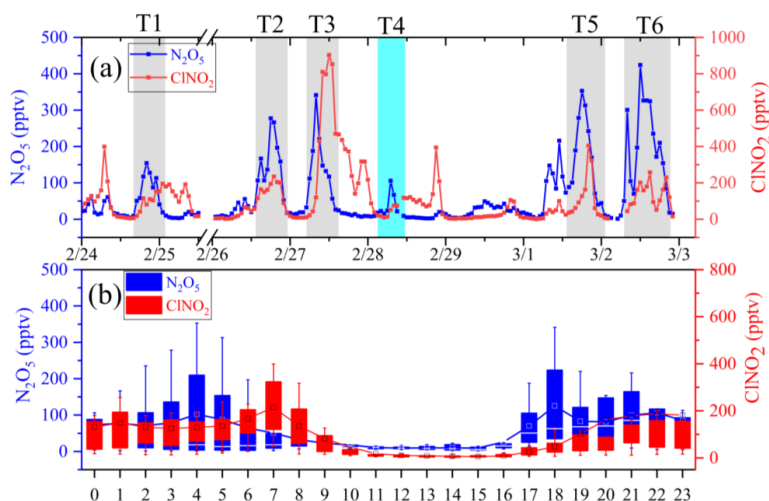
Scenario	Case	Aerosol Schemes		Ground Chemistry Model	Anthropogenic chlorine emissions
		Bertram09	Yu20		
B1	BT09_A	✓			✓
Y0	YU20_A		✓		NO
Y1	YU20_A_nohetN <sub>2</sub> O <sub>5</sub>				✓
Y2	YU20_A_chl		✓		✓
Y3	YU20_A_G_chl		✓	✓	✓
Y4	YU20_A_G_chl_nohv		✓	(turn off the photolysis reaction of ClNO <sub>2</sub> )	✓

212

### 213 3. Result and discussion

#### 214 3.1 Overview of Wintertime Observations

215



216

217 **Figure 2** Field observations of N<sub>2</sub>O<sub>5</sub> and ClNO<sub>2</sub> at the DLS station from February 23  
218 to March 3, 2024. (a) Time series, (b) Diurnal variation.

219

220 The time series of N<sub>2</sub>O<sub>5</sub> and ClNO<sub>2</sub> concentrations is depicted in the Fig. 2 during  
221 the observation period. N<sub>2</sub>O<sub>5</sub> concentrations ranged from 0.76 to 424.15 pptv, with an  
222 average of 58.73 ± 83.37 pptv. ClNO<sub>2</sub> exhibited an average concentration of 102.64 ±  
223 146.43 pptv with a peak value of 902.45 pptv on the 27th, February. The peaks of N<sub>2</sub>O<sub>5</sub>  
224 and ClNO<sub>2</sub> exhibit synchronicity at certain time points during T1, T2, T3, T5, and T6.  
225 This phenomenon is attributed to the role of N<sub>2</sub>O<sub>5</sub> as a precursor to ClNO<sub>2</sub>, where  
elevated N<sub>2</sub>O<sub>5</sub> concentrations drive the chemical equilibrium toward ClNO<sub>2</sub> formation.



226 However, when the  $\text{N}_2\text{O}_5$  concentration was below the 120 pptv, no corresponding  
227  $\text{ClNO}_2$  peak was observed during T4. This discrepancy is mainly due to the hydrolysis  
228 of  $\text{N}_2\text{O}_5$  to form nitrate (R3) under low concentration conditions. The hydrolysis  
229 reaction of  $\text{N}_2\text{O}_5$  proceeds at a faster rate than its reaction with HCl, and the resulting  
230 nitric acid further stabilizes the reaction system. Fig. 2b presents the average daily  
231 variation patterns of these two species, with a general accumulation at night and rapid  
232 depletion during the day, and the similar temporal pattern over snow-covered areas has  
233 been widely reported in previous studies (Xia et al., 2020; Kulju et al., 2022; Jeong et  
234 al., 2023; Li et al., 2025). The average daily values of  $\text{N}_2\text{O}_5$  and  $\text{ClNO}_2$  were  $49.21 \pm$   
235  $37.51$  pptv and  $56.51 \pm 30.70$  pptv, respectively.  $\text{ClNO}_2$  concentrations exhibited a  
236 pronounced diurnal cycle, accumulating at night and reaching a maximum of 113.45  
237 pptv around 7:00 AM. Following sunrise, rapid photolysis of  $\text{ClNO}_2$  led to a sharp  
238 decline in its concentrations during daylight hours, accompanied by the release of  
239 chlorine atoms.

### 240 3.2 Model performance of the updated heterogeneous $\text{N}_2\text{O}_5$ chemistry on 241 aerosol/ground surfaces

#### 242 3.2.1 Comparative analysis of aerosol schemes on heterogeneous $\text{N}_2\text{O}_5$ reaction

243 This study compared the performance of the BT09 and YU20 aerosol schemes  
244 within the CAMx model during snow-covered periods. The YU20 scheme  
245 demonstrated significant improvements in the statistical indicators for  $\text{N}_2\text{O}_5$  and  $\text{ClNO}_2$   
246 compared to the BT09 scheme (Table S3). For  $\text{N}_2\text{O}_5$ , the MB decreased from 114.62 to  
247 69.66, the NMB from 1.92 to 1.16, and the RMSE from 201.39 to 139.03, while the  
248 IOA increased from 0.49 to 0.61. Similarly, for  $\text{ClNO}_2$ , the MB decreased from -29.28  
249 to -16.08, the NMB from -0.28 to -0.16, the RMSE from 100.66 to 99.80, with the IOA  
250 from 0.81 to 0.84. The YU20 scheme is a set of parameter values derived from local  
251 observation data in China, making it more representative of the evolution of  
252 atmospheric chemical species in the region. Given the above enhancements, the YU20  
253 aerosol scheme was selected for use in subsequent scenario simulations.

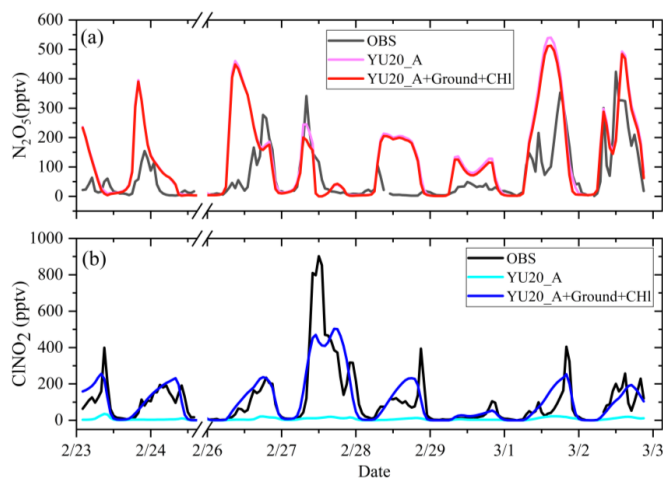
254 The parameters  $\gamma(\text{N}_2\text{O}_5)$  and  $\phi(\text{ClNO}_2)$  are critical parameters for understanding



255  $N_2O_5$  heterogeneous chemistry on aerosol surfaces. The BT09 scheme is believed to  
 256 overestimate the  $\gamma(N_2O_5)$  (Wagner et al., 2013) and  $\phi(CINO_2)$  (McDuffie et al., 2018).  
 257 Yang et al. (2022) further demonstrated that incorporating anthropogenic chlorine and  
 258 biomass burning emissions into the YU20 parameterization effectively enhanced  
 259  $\gamma(N_2O_5)$  values, emphasizing the advantage of localized schemes for improving model  
 260 accuracy (Yang et al., 2022). However, Xie et al. (2025) found that the BT09 scheme  
 261 outperformed YU20 at the Wangdu station in Hebei province of China under snow-free  
 262 conditions using the WRF-CAMx model. Similarly, Dai et al. (2020) evaluated the  
 263 emission of pCl from the South China Sea and also found that the BT09 aerosol scheme  
 264 better captured the peak value of  $CINO_2$  compared to the YU20 scheme.

265 In contrast, our study found that YU20 performed better than BT09 during snow-  
 266 covered conditions. This improvement can be attributed to the significant impact of  
 267 atmospheric humidity changes under snow cover conditions, along with an increase in  
 268 winter chlorine emissions in high-latitude regions. These factors together drove changes  
 269 in species concentrations (chloride ions, and nitrate ions) on aerosol surfaces during the  
 270 observation period, directly affecting the  $\gamma(N_2O_5)$  and  $\phi(CINO_2)$  values in the  $N_2O_5$   
 271 aerosol schemes (BT09 or YU20).

272 3.2.2 Comparison of model simulations with observation



273

274 **Figure 3** Comparison of simulated and observed values for YU20\_A (Y0) and  
 275 YU\_A\_G\_ChI (Y3) the DLS station in Northeast China: (a)  $N_2O_5$ , (b)  $CINO_2$ .



276 A comparison of atmospheric  $\text{N}_2\text{O}_5$  and  $\text{ClNO}_2$  concentrations before and after  
 277 model modification is presented in Fig. 3. In the Y0 scenario,  $\text{N}_2\text{O}_5$  concentrations  
 278 averaged  $141.81 \pm 148.62$  pptv, with a peak value of 540.37 pptv. In the Y3 scenario  
 279 with modified modeling,  $\text{N}_2\text{O}_5$  concentrations ranged from 0.0 to 513.03 pptv, with an  
 280 average value of  $33.58 \pm 143.92$  pptv. While the mean bias (MB) of  $\text{N}_2\text{O}_5$  decreased  
 281 from 64.10 pptv to 56.53 pptv, the normalized mean bias (NMB) from 0.98 % to 0.87%,  
 282 and the root mean square error (RMSE) from 123.17 pptv to 118.39 pptv, the index of  
 283 agreement (IOA) remained at 0.66 (Table 3). This suggests no significant improvement  
 284 in model accuracy, likely due to the relatively low re-emission rate of  $\text{N}_2\text{O}_5$  deposited  
 285 on the ground surface, which has a minimal impact on atmospheric  $\text{N}_2\text{O}_5$  concentrations.

286 In contrast, the revised model significantly improved the simulation of  $\text{ClNO}_2$ ,  
 287 particularly in capturing peak concentrations. In Y0 scenario, the average  $\text{ClNO}_2$   
 288 concentrations is  $7.73 \pm 6.96$  pptv with a peak value of 35.59 pptv. In contrast, the Y3  
 289 scenario showed an expanded range of 0.07 to 503.30 pptv and an increased average  
 290 concentration of  $110.30 \pm 117.45$  pptv. Additionally, the MB of  $\text{ClNO}_2$  improved from  
 291 -105.79 pptv to 2.66 pptv, the NMB increased from -0.93% to 0.02%, and the RMSE  
 292 decreased from 170.26 pptv to 88.28 pptv. The IOA also improved significantly, rising  
 293 from 0.39 to 0.86 (Table 3). These results demonstrate that incorporating chlorine  
 294 emissions and surface  $\text{N}_2\text{O}_5$  chemical processes into the CAMx model substantially  
 295 enhanced the simulation accuracy for  $\text{ClNO}_2$ , while the impact on  $\text{N}_2\text{O}_5$  remained  
 296 limited.

297 Table 3 Statistical indicators for the simulation results of  $\text{N}_2\text{O}_5$  and  $\text{ClNO}_2$   
 298 between Y0 and Y3 scenarios.

Species	Schemes	MB (pptv)	NMB (%)	RMSE (pptv)	IOA
$\text{N}_2\text{O}_5$	Y0	64.10	0.98	123.17	0.66
	Y3	56.53	0.87	118.39	0.66
$\text{ClNO}_2$	Y0	-105.78	-0.93	170.26	0.39
	Y3	2.66	0.02	88.28	0.86

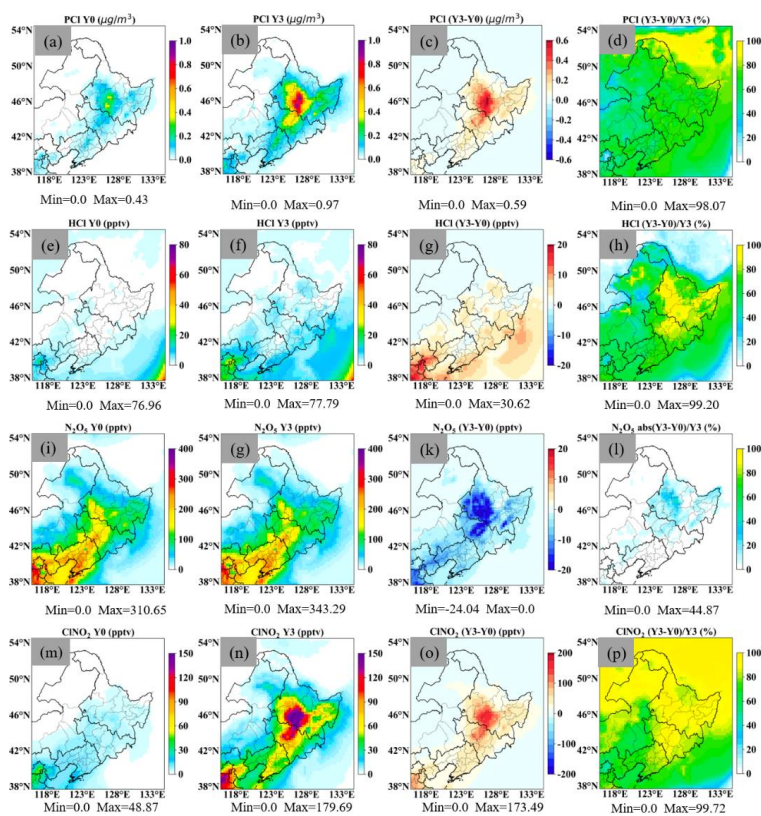
299

### 300 3.2.3 The Spatial impacts of chlorine emissions and chlorine chemistry

301 In northern regions of China, residential heating typically extends from early



302 November through March of the following year. During this period, coal combustion  
303 releases substantial quantities of particulate chloride (PCl) and HCl into the atmosphere  
304 (Liu et al., 2018). To assess the impact of model modifications, we further examined  
305 the spatial concentration differences and ratios of PCl, HCl, N<sub>2</sub>O<sub>5</sub>, and ClNO<sub>2</sub> between  
306 Y0 and Y3 (Fig. 4). The spatial concentration differences (e.g., Y3–Y0) are used to  
307 quantify the magnitude of changes in simulated pollutant concentrations between  
308 different scenarios, while contribution ratios (e.g., (Y3–Y0)/Y3) are employed to assess  
309 the relative contributions of model modifications. For PCl and HCl, peak spatial  
310 concentrations in the Y0 scenario reached 0.43 μg/m<sup>3</sup> and 76.96 pptv, respectively. In  
311 the Y3 scenario, these ranges increased to 0–0.97 μg/m<sup>3</sup> for PCl and 0–77.79 pptv for  
312 HCl. The spatial differences in PCl concentrations between the Y0 and Y3 scenarios  
313 ranged from 0 to 0.59 μg/m<sup>3</sup>, with the most significant differences observed in  
314 Heilongjiang and Liaoning provinces, where the contribution rate was approximately  
315 72%. Meanwhile, the spatial differences in HCl concentrations between the Y0 and Y3  
316 scenarios ranged from 0 to 8.21 pptv with the highest contribution rate was 99.20% in  
317 Heilongjiang province. Regarding N<sub>2</sub>O<sub>5</sub> and ClNO<sub>2</sub>, the N<sub>2</sub>O<sub>5</sub> concentration peaked at  
318 310.65 pptv in the Y0 scenario, while the maximum spatial concentration increased to  
319 343.29 pptv in the Y3 scenario. The spatial differences in N<sub>2</sub>O<sub>5</sub> between the Y0 and Y3  
320 scenarios ranged from -24.04 to 0.0 pptv (Fig. 4k) with a maximum contribution ratio  
321 of 44.87%, indicating net consumption of N<sub>2</sub>O<sub>5</sub>. ClNO<sub>2</sub> concentrations peaked at  
322 116.82 pptv in the Y0 scenario and increased to 179.69 pptv in the Y3 scenario. Spatial  
323 differences of ClNO<sub>2</sub> between the Y0 and Y3 scenarios ranged from 0 to 173.49 pptv  
324 (Fig. 4o) with the contribution rate of ClNO<sub>2</sub> concentrations exceeding 90% in most  
325 simulated regions. These findings highlight the significant impact of incorporating  
326 anthropogenic chlorine emissions and revised chlorine chemical reaction mechanisms  
327 on regional ClNO<sub>2</sub> concentrations.



328  
 329 **Figure 4** The spatial distribution of the impact of chlorine emissions and chlorine  
 330 chemical reactions on pollutants (PCI, HCl,  $\text{N}_2\text{O}_5$ , and  $\text{ClNO}_2$ ). (Y0:YU20\_A;  
 331 Y3:YU20\_A\_G\_chl.)  
 332

333 3.3 The relative contribution of chlorine emissions and ground surface  
 334 chlorine chemistry

335 The comprehensive impact of anthropogenic chlorine emissions and  
 336 heterogeneous chemical reactions of surface  $\text{N}_2\text{O}_5$  on  $\text{ClNO}_2$  concentration had been  
 337 quantitatively evaluated by comparing Y0 and Y3 scenarios. Here, we further analyzed  
 338 the individual effects of chlorine emissions and surface chemical reactions separately.

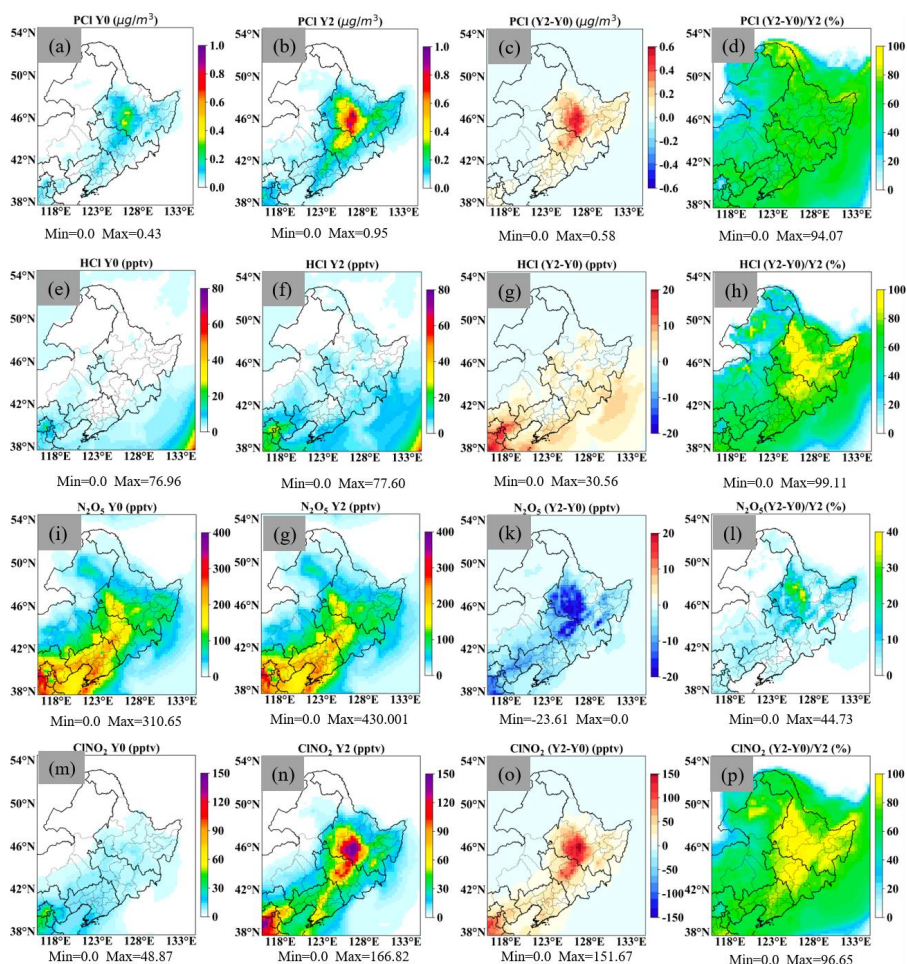
339 3.3.1 The impact of chlorine emission on  $\text{ClNO}_2$

340 To isolate the contribution of anthropogenic chlorine emissions, the Y0 and Y2  
 341 scenarios were established. In the Y2 scenario, the spatial concentrations of PCI and  
 342 HCl ranged from 0.0 to 0.95  $\mu\text{g}/\text{m}^3$  and 0.0 to 77.60 pptv, respectively. The spatial



343 differences in PCI between the Y0 and Y2 scenarios ranged from 0.0 to 0.58 pptv (Fig.  
344 5), with an average contribution ratio of 61.02%. Similarly, the spatial differences in  
345 HCl concentrations between the Y0 and Y2 scenarios ranged from 0 to 30.56 pptv, with  
346 the highest contribution rate of 99.11% observed in Heilongjiang Province, China.  
347 Notably, the peak ClNO<sub>2</sub> concentration in the Y2 scenario reached 166.82 pptv, with a  
348 maximum difference of 151.67 pptv. In most regions of northeastern China, ClNO<sub>2</sub>  
349 contributions exceeded 50%.

350 For snow-free conditions, Liu et al. (2018) first utilized the ACEIC chlorine  
351 emission inventory in the Community Multi-scale Air Quality (CMAQ) modeling  
352 system and found that anthropogenic chlorine emissions contributed approximately 100  
353 pptv to ClNO<sub>2</sub> concentrations, with a contribution range of 30%–50%. Similarly, Hong  
354 et al. (2020) using the CMAQ model with ACEIC inventory, further reported that the  
355 maximum contribution of chlorine emissions to ClNO<sub>2</sub> ranged from 50 to 100 pptv in  
356 Liaoning Province, corresponding to a contribution rate of 20%–50%. In contrast, the  
357 simulated contribution concentration range in Jilin and Heilongjiang Provinces was  
358 only 10–50 pptv, with a corresponding contribution rate of 10%–20%. However, under  
359 snow-covered conditions in this study, simulations using the CAMx model and an  
360 updated ACEIC inventory yielded ClNO<sub>2</sub> concentrations ranging from 0 to 151.67 pptv,  
361 with a contribution range of 50%–90%. This suggests that snow cover with higher  
362 albedo plays a significant role in the photochemistry of the ClNO<sub>2</sub> generation.  
363 Additionally, differences in air quality models and simulation periods may also  
364 contribute to the variations observed among these studies.



365

366

367

**Figure 5** The spatial distribution of the impact of chlorine emissions on pollutants (PCI, HCl, N<sub>2</sub>O<sub>5</sub>, and ClNO<sub>2</sub>). (Y0:YU20\_A; Y2:YU20\_A\_chl.)

368

### 3.3.2 The impact of ground surface chlorine chemistry on ClNO<sub>2</sub>

369

370

371

372

373

The existing air quality models typically underestimate ClNO<sub>2</sub> concentrations compared to observed values, suggesting the presence of unknown sources. To address this gap, we further incorporated two new ground surface chemical reactions including ClNO<sub>2</sub> production and consumption reactions (Table 2) into a 3D air quality model to investigate the contribution of these unknown ClNO<sub>2</sub> sources.

374

375

376

Fig. 6 presents the simulated spatial distributions of monthly mean, nighttime monthly mean, and daytime monthly mean ClNO<sub>2</sub> concentrations, along with their corresponding contribution ratios from ground surface chemistry. The spatial



377 differences in  $\text{ClNO}_2$  between the Y2 and Y3 scenarios ranged from 0.0 to 38.96 pptv,  
378 with the contribution ratios of up to 48.20% observed in Heilongjiang, Jilin, and the  
379 northeastern regions of Liaoning Province (Fig. 6c and 6d). The higher albedo of snow  
380 can facilitate the surface photochemical reactions and lead to rapid  $\text{ClNO}_2$  photolysis  
381 (Chen et al., 2019), which explains significant differences in the concentration of  
382  $\text{ClNO}_2$  between daytime and nighttime. During the daytime,  $\text{ClNO}_2$  concentrations in  
383 both the Y2 and Y3 scenarios ranged from 0 to 70.60 pptv. The maximum spatial  
384 difference in  $\text{ClNO}_2$  between the Y2 and Y3 scenarios was 7.51 pptv, with monthly  
385 average contribution ratios reaching up to 23.02% in the eastern regions of Heilongjiang  
386 and Jilin Provinces. In contrast, nighttime  $\text{ClNO}_2$  concentrations exhibited an  
387 accumulation trend. Scenarios Y2 and Y3 simulated maximum nighttime  $\text{ClNO}_2$   
388 concentrations of 271.07 pptv and 310.04 pptv, respectively. The nighttime spatial  
389 maximum difference (72.14 pptv) was approximately ten times greater than that  
390 observed during the day, with a contribution ratio of around 92% in Heilongjiang and  
391 Jilin Provinces.

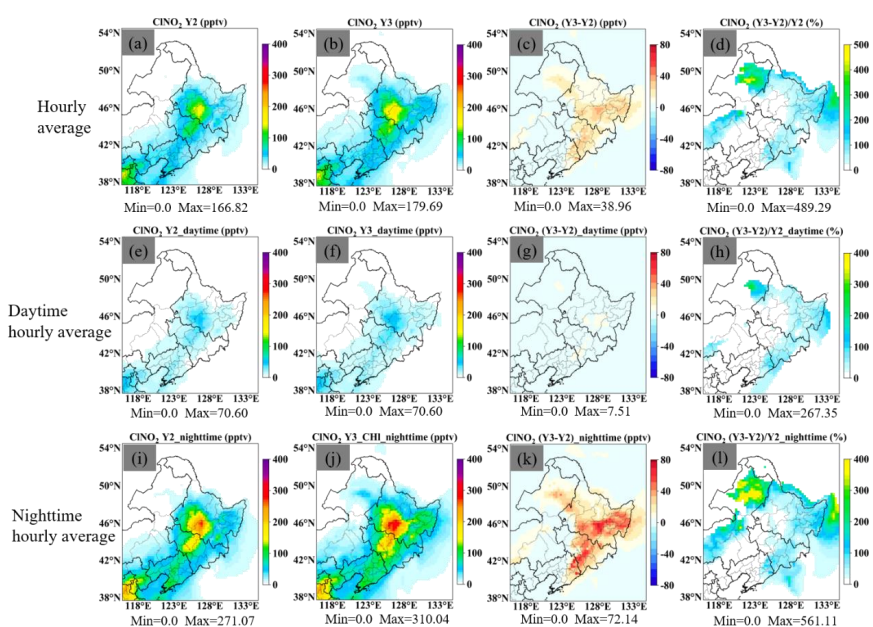
392 The flux exchange between ground surface chemical processes and the atmosphere  
393 is a critical component of atmospheric chemistry. Pollutants deposited on surfaces (soil,  
394 snow, vegetation, and buildings) can also undergo heterogeneous chemical reactions.  
395 Snow, in particular, provides a larger reaction interface for heterogeneous chemical  
396 while low temperatures influence chemical equilibria and increase atmospheric  
397 moisture content, favoring gas deposition processes (McNamara et al., 2021).  
398 Consequently, higher  $\text{ClNO}_2$  and  $\text{N}_2\text{O}_5$  concentrations are observed during winter  
399 compared to summer (Xia et al., 2021), primarily due to elevated  $\text{N}_2\text{O}_5$  levels enhancing  
400  $\text{ClNO}_2$  production, while lower winter temperatures favor the equilibrium shift of the  
401  $\text{N}_2\text{O}_5\text{-NO}_3$  reaction toward  $\text{N}_2\text{O}_5$  formation. Additionally, longer winter nights in high  
402 latitudes facilitate  $\text{N}_2\text{O}_5$  accumulation under dark conditions (Wagner et al., 2013).

403 The  $\text{ClNO}_2$  yield and flux variations serve as key indicators for assessing the  
404 significance of surface heterogeneous chemical processes. During the snow-covered  
405 periods, the  $\phi(\text{ClNO}_2)$  values are higher compared to snow free periods, ranging from  
406 0.065 to 1.00 during most winter months in the Northern Hemisphere (Table 4). Notably,



407 over snow surfaces, Wang et al. (2020) and Jeong et al. (2023) reported the  $\phi(\text{ClNO}_2)$   
 408 values even exceeding 0.80 during winter.

409 From the perspective of  $\text{ClNO}_2$  flux variations, McNamara et al. (2021) conducted  
 410 vertical gas profile observations and snow chamber experiments in Kalamazoo,  
 411 Michigan, reporting a daily averaged  $\text{ClNO}_2$  flux of  $3 \times 10^7$  molecules  $\text{cm}^{-2} \text{s}^{-1}$  over  
 412 snow-covered surfaces, compared to a negative flux of  $-24 \times 10^7$  molecules  $\text{cm}^{-2} \text{s}^{-1}$   
 413 over snow-free surfaces. Jeong et al. (2023) further integrated a one-dimensional  
 414 atmospheric boundary layer model with snow modules to investigate the vertical  
 415 distribution and impact of urban snow cover on  $\text{ClNO}_2$  emissions in Kalamazoo,  
 416 Michigan. Their findings showed that the  $\text{ClNO}_2$  flux was positive on snow-covered  
 417 nights, averaging  $3.7 \times 10^8$  molecules  $\text{cm}^{-2} \text{s}^{-1}$ , but turned negative on snow-free nights,  
 418 averaging  $-(2.8 \times 10^9)$  molecules  $\text{cm}^{-2} \text{s}^{-1}$ . These findings indicate that under snow-  
 419 covered conditions, the flux of  $\text{ClNO}_2$  is positive, whereas under snow-free conditions,  
 420 it turns negative. Furthermore, the positive flux of  $\text{ClNO}_2$  during nighttime snow  
 421 conditions is significantly higher than the daily average flux.



422

423 **Figure 6** The quantitative contribution of ground surface chemistry to hourly  
 424 atmospheric  $\text{ClNO}_2$  over northeastern China. (Y2:YU20\_A\_chl;  
 425 Y3:YU20\_A\_G\_chl.)



426 As mentioned above, snow-covered ground surfaces exhibit higher  $\phi(\text{ClNO}_2)$   
 427 values and larger positive  $\text{ClNO}_2$  fluxes (Jeong et al., 2023; Kulju et al., 2021;  
 428 McNamara et al., 2021), particularly at night. In this study, we further integrated the  
 429 surface chemistry module into the 4D Eulerian model of CAMx, establishing a link for  
 430 flux exchange between the ground surfaces and the atmosphere. This integration  
 431 provides a bridge to explore the spatiotemporal variations in  $\text{ClNO}_2$  concentration and  
 432 allows for a more nuanced quantification of the impacts of chlorine chemistry on  
 433 atmospheric oxidizing capacity and regional air quality.

434 **Table 4.** Summary of literature on the yield of  $\text{ClNO}_2$  in winter

Period	Site	Surface	Method	$\phi(\text{ClNO}_2)$	Reference
February to March 2015	Eastern, U.S.	Aerosol	Box model	$\phi(\text{ClNO}_2) = 0.138$	(McDuffie et al., 2018)
February to March 2011	Northern Denver, U.S.	Aerosol	Box model	$\phi(\text{ClNO}_2) = 0.065$	(Wagner et al., 2013)
7 March to 8 April 2018	Mt. Tai, China	Aerosol	Box model	$\phi(\text{ClNO}_2) = 0.47$	
6 January to 1 February 2018	Beijing, China (Urban)	Aerosol	Box model	$\phi(\text{ClNO}_2) = 0.28$	(Xia et al., 2021)
9 December to 31 December 2017	Wangdu, China (Rural)	Aerosol	Box model	$\phi(\text{ClNO}_2) < 0.10$	
February 2016	Ann Arbor, MI, U.S.	Snowpack	$k_{\text{N}_2\text{O}_5}$ from steady state approximation	~257 K: $\phi(\text{ClNO}_2) > 0.90$ 270 - 272 K: $\phi(\text{ClNO}_2):$ 0.5~0.75 < 273K: $\phi(\text{ClNO}_2) = 0.05$	(Wang et al., 2020)
12 January to 24 February 2018	Kalamazoo, Michigan, U.S.	Snowpack	$k_{\text{N}_2\text{O}_5}$ from steady state approximation	$\phi(\text{ClNO}_2) > 0.80$	(Jeong et al., 2023)

435

### 436 3.4 Contribution of Reactive Chlorine to AOC, $\text{PM}_{2.5}$ , and $\text{O}_3$

#### 437 3.4.1 Contribution on Atmospheric Oxidizing Capacity (AOC)

438 According to previous studies (Lu et al., 2014; Zhu et al., 2022), the incorporation  
 439 of chlorine chemical reactions can enhance the AOC. The spatial concentrations of  
 440 oxidizing species (OH,  $\text{HO}_2$ , and  $\text{RO}_2$ ) in scenarios Y0, Y1, Y2, and Y3 are shown in  
 441 (Fig. S4). The contributions of anthropogenic chlorine emissions and  $\text{N}_2\text{O}_5$   
 442 heterogeneous chemistry under different conditions are illustrated in Fig. 7. Note that



443 Y3-Y0, Y2-Y1, and Y3-Y2 represent contributions from N<sub>2</sub>O<sub>5</sub> heterogeneous chemistry,  
444 aerosol surface heterogeneous chemistry, and ground surface heterogeneous chemistry,  
445 denoted as Chl\_het\_N<sub>2</sub>O<sub>5</sub>\_a+g, Het\_N<sub>2</sub>O<sub>5</sub>\_a, and Het\_N<sub>2</sub>O<sub>5</sub>\_g, respectively.

446 In the Chl\_het\_N<sub>2</sub>O<sub>5</sub>\_a+g scenario, the maximum OH concentration difference  
447 reached  $53.12 \times 10^6 \text{ cm}^{-3}$  with a maximum relative contribution of 7.59%. This result  
448 is consistent with Wang et al. (2020), who reported a 6% contribution of anthropogenic  
449 chlorine emissions to the AOC in Northeast China for 2014 (Wang et al., 2020). The  
450 spatial concentration difference in RO<sub>2</sub> ranged from  $-(15.78 \times 10^8) \text{ cm}^{-3}$  to  $11.45 \times 10^8$   
451  $\text{cm}^{-3}$  with a maximum relative contribution of 6.56%. The HO<sub>2</sub> concentration was more  
452 regionalized where it primarily concentrated in coastal areas of the Beijing-Tianjin-  
453 Hebei region and the Bo Sea, with the range of  $-(67.73 \times 10^8) \text{ cm}^{-3}$  to  $2.52 \times 10^8 \text{ cm}^{-3}$   
454 and a relative contribution of approximately 3% in Northeast China.

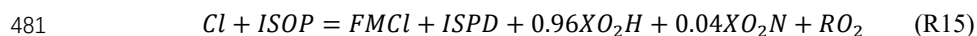
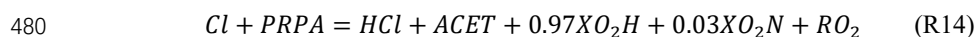
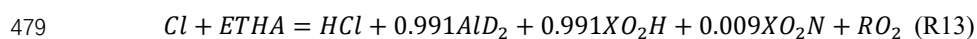
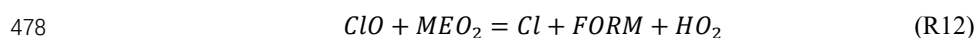
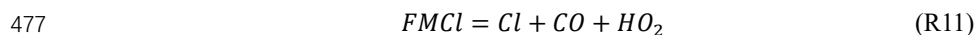
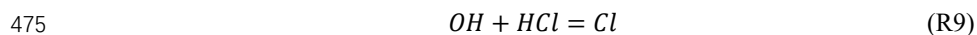
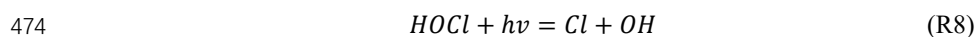
455 In the Het\_N<sub>2</sub>O<sub>5</sub>\_a scenario, the spatial OH concentration difference ranged from  
456  $-(2.12 \times 10^6) \text{ cm}^{-3}$  to  $27.14 \times 10^6 \text{ cm}^{-3}$  with a maximum relative contribution of 6.34%.  
457 The maximum HO<sub>2</sub> concentration difference ( $13.05 \times 10^6 \text{ cm}^{-3}$ ) exceeded that simulated  
458 in the Chl\_het\_N<sub>2</sub>O<sub>5</sub>\_a+g scenario, and the RO<sub>2</sub> difference range  $-(100.51 \times 10^8) \text{ cm}^{-3}$  to  
459  $4.17 \times 10^8 \text{ cm}^{-3}$  was also larger than in the Chl\_het\_N<sub>2</sub>O<sub>5</sub>\_a+g scenario.

460 In the Het\_N<sub>2</sub>O<sub>5</sub>\_g scenario, the OH concentration difference ranged from  $-(1.73$   
461  $\times 10^6) \text{ cm}^{-3}$  to  $52.22 \times 10^6 \text{ cm}^{-3}$ , and the contribution regions were primarily  
462 concentrated in Heilongjiang Province and the four eastern regions of Inner Mongolia  
463 with a maximum relative contribution of 7.37%. The maximum HO<sub>2</sub> contribution was  
464 5.98%, while the RO<sub>2</sub> contribution was the smallest at 1.99%. The results illustrate that  
465 under snow cover conditions, chlorine chemistry generally promotes OH generation,  
466 inhibits RO<sub>2</sub> production, and has varying effects on HO<sub>2</sub> production, inhibiting it in  
467 Chifeng city while promoting it in other regions of Northeast China (Fig. 7).

468 The greater spatial distribution differences observed in Het\_N<sub>2</sub>O<sub>5</sub>\_a compared to  
469 Chl\_het\_N<sub>2</sub>O<sub>5</sub>\_a+g can be attributed to the CB6r2h-lts chemical mechanism, which  
470 includes 22 gas-phase chlorine reactions, eight of which (R8-R15) directly impact the  
471 generation and removal of OH, HO<sub>2</sub>, and RO<sub>2</sub>. The analysis reveals that the  
472 Het\_N<sub>2</sub>O<sub>5</sub>\_a scenario had the most significant impact, followed by Chl\_het\_N<sub>2</sub>O<sub>5</sub>\_a+g,

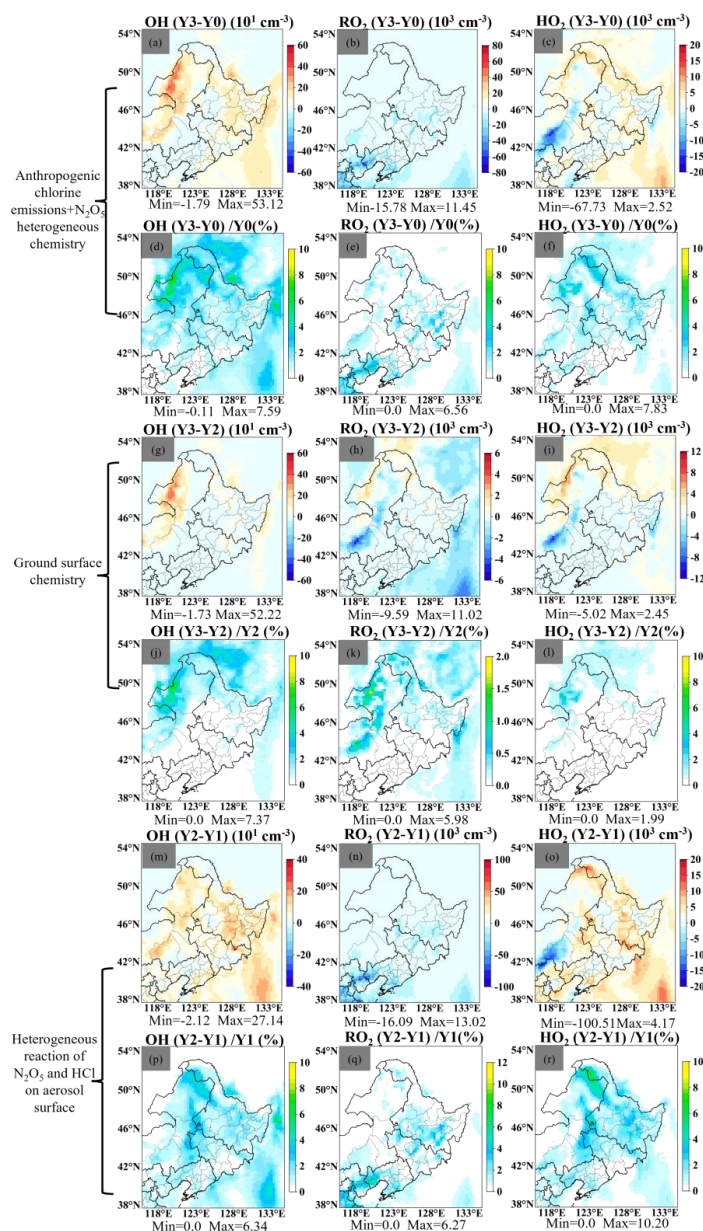


473 while the contribution of  $\text{Het\_N}_2\text{O}_5\text{\_g}$  was relatively minor.



482 Where FMCL denotes formyl chloride ( $\text{HC(O)Cl}$ );  $\text{MEO}_2$  represents the methyl peroxy  
483 radical;  $\text{AID}_2$  refers to acetaldehyde and higher aldehydes;  $\text{XO}_2\text{H}$  indicates NO-to- $\text{NO}_2$   
484 converting peroxy radicals from HCs;  $\text{XO}_2\text{N}$  signifies NO-to-organic nitrate converting  
485 peroxy radicals; ISPD represents Isoprene product / Isoprene-derived peroxy radical;  
486 FORM denotes formaldehyde; ACET indicates acetone; and ISOP represents isoprene.

487



488

489

490

491

492

493

494

495

**Figure 7** The quantitative contribution of different pathways of chlorine chemistry on atmospheric oxidizing capacity. (a-f) Chl\_het\_N<sub>2</sub>O<sub>5</sub>\_a+g: anthropogenic chlorine emissions+N<sub>2</sub>O<sub>5</sub> heterogeneous chemistry (Y3-Y0); (g-l) Het\_N<sub>2</sub>O<sub>5</sub>\_g: ground surface chemistry (Y3-Y2); (m-r) Het\_N<sub>2</sub>O<sub>5</sub>\_a: heterogeneous reactions of N<sub>2</sub>O<sub>5</sub> and HCl on aerosol surface (Y2-Y1).

### 3.4.2 Contribution on PM<sub>2.5</sub>

Chlorine emissions and the associated chlorine chemical reactions significantly



496 influence AOC, the formation of particulate matter, and ozone levels. Fig. S5 presents  
497 the spatial concentration distributions of these species with concentration ranges of 0-  
498 128.64  $\mu\text{g}/\text{m}^3$  for  $\text{PM}_{2.5}$ , 0-16.94  $\mu\text{g}/\text{m}^3$  for  $\text{PNH}_4$ , 0-13.06  $\mu\text{g}/\text{m}^3$  for  $\text{PSO}_4$ , and 0-47.53  
499  $\mu\text{g}/\text{m}^3$  for  $\text{PNO}_3$ , respectively. Fig. 8 exhibited the differences and contribution ratios  
500 of scenarios (Y3-Y0), (Y2-Y1), and (Y3-Y2) on  $\text{PM}_{2.5}$  and its components ( $\text{PNH}_4$ ,  $\text{PSO}_4$ ,  
501 and  $\text{PNO}_3$ ), respectively.

502 In the `Chl_het_N2O5_a+g` scenario, chlorine chemistry suppressed  $\text{PM}_{2.5}$   
503 formation in the eastern regions of Northeast China with a maximum suppression of  
504 1.94  $\mu\text{g}/\text{m}^3$ . Conversely, chlorine chemistry promoted  $\text{PM}_{2.5}$  formation in most regions  
505 of Heilongjiang, Jilin, and Liaoning Provinces with a significant increase of 3.65  $\mu\text{g}/\text{m}^3$   
506 and a maximum relative contribution of 15.34%. The simulation results show that  
507 chlorine addition promoted the formation of  $\text{PNH}_4$  (increased by 0.73  $\mu\text{g}/\text{m}^3$ ) and  $\text{PSO}_4$   
508 (increased by 0.37  $\mu\text{g}/\text{m}^3$ ) which were primarily concentrated in urban areas such as  
509 Harbin and Changchun. In contrast,  $\text{PNO}_3$  was suppressed, with a minimum difference  
510 value of -1.78  $\mu\text{g}/\text{m}^3$  and a corresponding relative contribution of 23.77%.

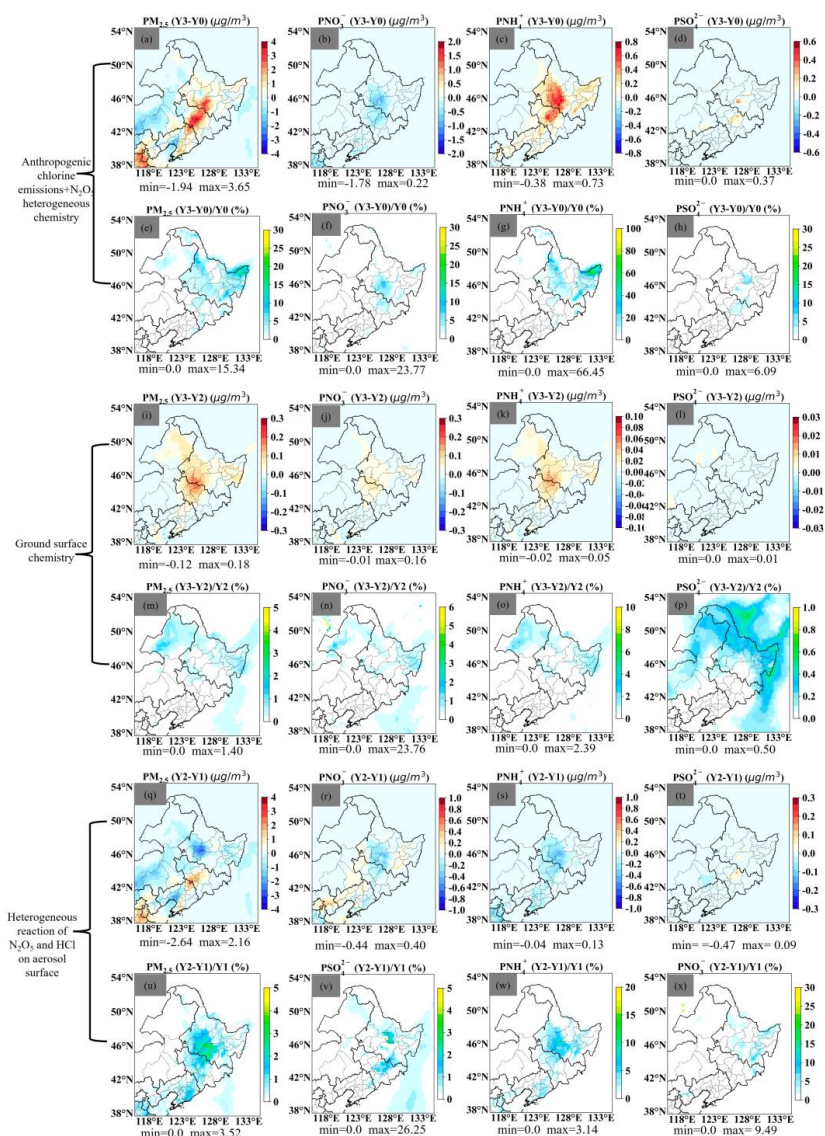
511 In the `Het_N2O5_a` scenario,  $\text{PM}_{2.5}$  was inhibited in the eastern regions of  
512 Heilongjiang and Liaoning Provinces, while an increase was observed in certain areas  
513 of Jilin Province, with concentration differences ranging from -2.64 to 2.16  $\mu\text{g}/\text{m}^3$  and  
514 a maximum contribution of 3.52%. Aerosol surface heterogeneous chemistry inhibited  
515  $\text{PNH}_4$  and  $\text{PNO}_3$  formation across most of the central and northeastern regions, with  
516 maximum relative contributions of 3.14% and 26.25%, respectively. The spatial  
517 concentration difference in  $\text{PSO}_4^{2-}$  was not significant in the Northeast region with the  
518 maximum value of 0.09  $\mu\text{g}/\text{m}^3$ .

519 In the `Het_N2O5_g` scenario, the formations of  $\text{PM}_{2.5}$ ,  $\text{PNO}_3$ ,  $\text{PNH}_4$ , and  $\text{PSO}_4^{2-}$   
520 were enhanced, with maximum differences of 0.18  $\mu\text{g}/\text{m}^3$ , 0.16  $\mu\text{g}/\text{m}^3$ , 0.05  $\mu\text{g}/\text{m}^3$ , and  
521 0.01  $\mu\text{g}/\text{m}^3$ , respectively. Compared to `Chl_het_N2O5_a+g` and `Het_N2O5_a`, the spatial  
522 concentration difference in `Het_N2O5_g` was relatively minor for these species.

523 In the `Het_N2O5_g` scenario, the impact on particulate matter is relatively small,  
524 primarily due to two factors: (1) the concentration of re-emitted species was low, and



525 the species involved were limited; and (2) highly oxidizing species such as HCl and  
 526 ClNO<sub>2</sub> in rapidly decomposed into other chlorides within the snow, preventing their  
 527 release into the atmosphere as oxidants and leading to a net loss of chlorine.  
 528 Additionally, an analysis of ClNO<sub>2</sub> photolysis in snow cover revealed a maximum  
 529 consumption value of 2.88 pptv, with a monthly average maximum concentration of  
 530 38.96 pptv on the ground, accounting for approximately 7.40% (Fig. S6).



531

532 **Figure 8** The quantitative contribution of different pathways of chlorine chemistry on



533  $PM_{2.5}$ , and its chemical components. (a-h) Chl\_het\_N<sub>2</sub>O<sub>5</sub>\_a+g: anthropogenic  
534 chlorine emissions+N<sub>2</sub>O<sub>5</sub> heterogenous chemistry (Y3-Y0); (i-p) Het\_N<sub>2</sub>O<sub>5</sub>\_g: ground  
535 surface chemistry (Y3-Y2); (q-x) Het\_N<sub>2</sub>O<sub>5</sub>\_a: heterogenous reactions of N<sub>2</sub>O<sub>5</sub> and  
536 HCl on aerosol surface (Y2-Y1).

### 537 3.4.3 Contribution on MDA8 O<sub>3</sub>

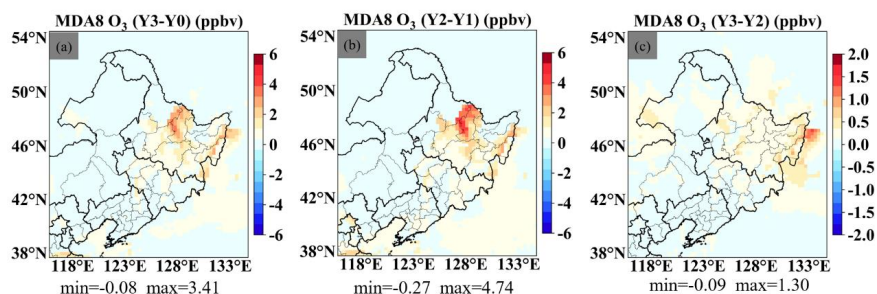
538 The anthropogenic chlorine emissions and N<sub>2</sub>O<sub>5</sub> heterogeneous chemistry can  
539 significantly enhance ozone levels. Previous studies have quantified this effect: Wang  
540 et al. (2020) reported that anthropogenic chlorine emissions increased the maximum  
541 daily 8-hour average (MDA8) O<sub>3</sub> concentration by 1.70 ppbv while Yi et al. (2023)  
542 found a 6.70 ppbv increase in winter MDA8 O<sub>3</sub> concentration in the Yangtze River  
543 Delta (YRD) region due to updates in chlorine chemistry processes. Furthermore, Yang  
544 et al. (2022) demonstrated that incorporating the anthropogenic chlorine emissions with  
545 biomass burning emissions and updating the parameterization of heterogeneous N<sub>2</sub>O<sub>5</sub>  
546 and Cl related chemistries, including adjustments of  $\gamma(N_2O_5)$  and  $\phi(CINO_2)$ , led to a 4.5  
547 ppbv increase in the MDA8O<sub>3</sub> concentration over China (Yang et al., 2022). In this  
548 study, the maximum difference in monthly mean MDA8 O<sub>3</sub> reached 3.41 ppbv (Fig. 9a),  
549 which

550 is smaller than the value observed (4.74 ppbv) in the Het\_N<sub>2</sub>O<sub>5</sub>\_a scenario. This  
551 difference is primarily attributed to the adding of chlorine emissions, which suppresses  
552 atmospheric oxidation. For example, the maximum difference concentrations of RO<sub>2</sub>  
553 and HO<sub>2</sub> in Het\_N<sub>2</sub>O<sub>5</sub>\_a are  $13.02 \times 10^8 \text{ cm}^{-3}$  and  $10.20 \times 10^8 \text{ cm}^{-3}$ , respectively, while  
554 in Chl\_het\_N<sub>2</sub>O<sub>5</sub>\_a+g, they are  $11.45 \times 10^8 \text{ cm}^{-3}$  and  $2.52 \times 10^8 \text{ cm}^{-3}$ , respectively (Fig.  
555 7). The maximum contribution concentration of surface heterogenous processes  
556 Het\_N<sub>2</sub>O<sub>5</sub>\_g to ozone was 1.30 ppbv (Fig. 9c).

557 To fully understand the dynamic exchange processes between the atmosphere and  
558 the ground surfaces, it is essential to quantify the mass of chemical species deposited  
559 on various surfaces, such as snow, vegetation, buildings, and soil, which provide  
560 sufficiently large reaction interfaces. Incorporating these deposition processes into the  
561 air quality models will offer a more comprehensive understanding of ground surface-  
562 atmosphere interactions and their impact on atmospheric chemistry. However, the  
563 current ground surface chemistry module remains relatively simplified, primarily



564 focusing on the re-emission of species into the atmosphere from predefined reactions.  
565 To more accurately represent the full impact of surface chemistry on atmospheric  
566 processes, further development and refinement of the ground surface module are  
567 necessary.



568

569 **Figure 9** The quantitative contribution of different pathways of chlorine chemistry on  
570 O<sub>3</sub>. (a) Chl\_het\_N<sub>2</sub>O<sub>5</sub>\_a+g: anthropogenic chlorine emissions+N<sub>2</sub>O<sub>5</sub> heterogeneous  
571 chemistry (Y3-Y0); (b) Het\_N<sub>2</sub>O<sub>5</sub>\_a: heterogeneous reactions of N<sub>2</sub>O<sub>5</sub> and HCl on  
572 aerosol surface (Y2-Y1); (c) Het\_N<sub>2</sub>O<sub>5</sub>\_g: ground surface chemistry (Y3-Y2).

#### 573 4. Conclusions

574 The mechanisms of heterogeneous N<sub>2</sub>O<sub>5</sub> reactions and ClNO<sub>2</sub> photolysis in snow  
575 remain incompletely understood. In this study, we employed numerical simulations to  
576 compare two different aerosol parameterization schemes involving chlorine chemistry  
577 (BT09 and YU20) and incorporated newly heterogeneous N<sub>2</sub>O<sub>5</sub> reactions on ground  
578 surfaces in WRF-CAMx model to assess their impacts on regional - scale atmosphere  
579 pollution under snow-covered conditions in Northeast China.

580 The observation results reveal distinct diurnal cycles of N<sub>2</sub>O<sub>5</sub> and ClNO<sub>2</sub>,  
581 characterized by nighttime accumulation during winter, followed by rapid photolysis  
582 after sunrise. The accumulation of N<sub>2</sub>O<sub>5</sub> concentrations promote ClNO<sub>2</sub> formation,  
583 whereas low N<sub>2</sub>O<sub>5</sub> levels (<120 pptv) favor hydrolysis to nitrate, preventing ClNO<sub>2</sub>  
584 peaks. Ground surface chemical processes accounted for about 28.36% of the simulated  
585 nighttime ClNO<sub>2</sub> accumulation in Northeastern China, which emphasizes the critical  
586 role of snow-covered surfaces in ClNO<sub>2</sub> production.

587 Furthermore, comparisons between different aerosol schemes demonstrated that  
588 the YU20 aerosol scheme outperforms the BT09 scheme in simulating N<sub>2</sub>O<sub>5</sub> and ClNO<sub>2</sub>  
589 concentrations within the CAMx model. Incorporating anthropogenic chlorine



590 emissions and surface  $\text{N}_2\text{O}_5$  heterogeneous chemistry significantly improved the  
591 model's performance on the simulated  $\text{ClNO}_2$  concentrations, reducing the RMSE from  
592 170.26 pptv to 88.28 pptv and increasing the IOA from 0.39 to 0.86. These processes  
593 increased hourly  $\text{PM}_{2.5}$  concentrations by up to  $3.65 \mu\text{g}/\text{m}^3$  (15.34%) and MDA8  $\text{O}_3$  by  
594 3.41 ppbv (5.68%), promoting particulate matter ( $\text{PNH}_4$  and  $\text{PSO}_4$ ) formation while  
595 suppressing  $\text{PNO}_3$ . Regarding regional impacts on the AOC Atmospheric Oxidizing  
596 Capacity,  $\text{PM}_{2.5}$ , and MDA8  $\text{O}_3$ , the contribution of  $\text{N}_2\text{O}_5$  heterogeneous chemistry on  
597 aerosol surfaces exceeded the combined effect of anthropogenic chlorine emissions and  
598 surface heterogeneous chemistry.

599 This study provides key insights into the role of the heterogenous chlorine  
600 chemistry in atmospheric processes over cold residential regions, and highlights  
601 unknown sources of  $\text{ClNO}_2$  on the ground surfaces during snow cover periods. From a  
602 3D air quality modeling perspective, quantifying the chemical deposition of  
603 atmospheric pollutants on diverse surfaces and integrating heterogenous chlorine  
604 related reaction processes into ground surface modules are crucial for accurately  
605 representing flux exchange between the ground and atmosphere. In the surface  
606 chemistry module, although the variation of rate constants for heterogeneous reactions  
607 at two snow layers is considered, further optimization is possible. By collecting snow  
608 samples at different depths in the field or conducting sensitive experiments in  
609 laboratory a long-term quantitative relationship among snow depth, total ion  
610 concentration ( $C_T$ ), and liquid brine layer fraction ( $f_{\text{brine}}$ ) can be established. This  
611 will allow for a more precise determination of the parameter values of  $\gamma(\text{N}_2\text{O}_5)$  and  
612  $\phi(\text{ClNO}_2)$  corresponding to different snow depths. Moreover, the snowmelt process  
613 requires special attention, as dynamic variations in liquid water content within snow/ice  
614 pores significantly affect heterogeneous reaction rate constants. Future studies should  
615 incorporate the numerical representation of these variations in models and evaluate the  
616 health impacts of regional atmospheric pollution driven by chemical exchanges  
617 between the atmosphere and the cryosphere.

618



## 619 Data availability

620 Snow satellite data were obtained from the National Snow and Ice Data Center  
621 (NSIDC) (<https://nsidc.org/data>), including snow cover fraction, snow density, and  
622 snow albedo. The air quality model employed CAMx version 7.10 or later  
623 (<https://www.camx.com/download/>). Observational data, simulation outputs, and the  
624 modified model code for N<sub>2</sub>O<sub>5</sub> heterogeneous chemistry have been uploaded to GitHub  
625 (<https://github.com/shengjinxie/Supplementary>).

626

## 627 Author contributions

628 Shengjin Xie, Xuelei Zhang, and Aijun Xiu designed the experiment. Shengjin Xie  
629 revised the code of CAMx and analyzed the data. Xuelei Zhang and Chao Gao provided  
630 suggestions for the model revision. Shengrui Tong, Hongmei Zhao, Shichun Zhang,  
631 Mengduo Zhang, and Stephen Dauda Yabo contributed to the writing and editing of the  
632 manuscript. Qianjie Chen provided the observational data in northeastern China.  
633 Yiming Liu and Siting Li supplied the anthropogenic chlorine emissions.

## 634 Competing interests

635 The contact author has declared that none of the authors has any competing interests.

## 636 Financial support

637 This project was partly supported by National Science Foundation of China  
638 (No.42371154, 42171142, 42305171); Youth Promotion Association of Chinese  
639 Academy of Sciences (2022230); The Excellent Young Scholars Fund of Jilin Province  
640 (No. 20240602020RC).

641

## 642 References

- 643 Apodaca, R. L., Huff, D. M., and Simpson, W. R.: The role of ice in N<sub>2</sub>O<sub>5</sub> heterogeneous hydrolysis at  
644 high latitudes, *Atmos. Chem. Phys.*, 8, 7451-7463, <https://doi.org/10.5194/acp-8-7451-2008>, 2008.
- 645 Bertram, T. H., and Thornton, J. A.: Toward a general parameterization of N<sub>2</sub>O<sub>5</sub> reactivity on aqueous  
646 particles: the competing effects of particle liquid water, nitrate and chloride, *Atmos. Chem. Phys.*, 9,  
647 8351-8363, <https://doi.org/10.5194/acp-9-8351-2009>, 2009.
- 648 Chen, Q., Edebeli, J., McNamara, S. M., Kulju, K. D., May, N. W., Bertman, S. B., Thanekar, S., Fuentes,



- 649 J. D., and Pratt, K. A.: HONO, particulate nitrite, and snow nitrite at a midlatitude urban site during  
650 wintertime, *ACS Earth Space Chem.*, 3, 811-822,  
651 <https://doi.org/10.1021/acsearthspacechem.9b00023>, 2019.
- 652 Dai, J., Liu, Y., Wang, P., Fu, X., Xia, M., and Wang, T.: The impact of sea-salt chloride on ozone  
653 through heterogeneous reaction with N<sub>2</sub>O<sub>5</sub> in a coastal region of south China, *Atmos. Environ.*, 236,  
654 117604, <https://doi.org/10.1016/j.atmosenv.2020.117604>, 2020.
- 655 Gaston, C. J., Thornton, J. A., and Ng, N. L.: Reactive uptake of N<sub>2</sub>O<sub>5</sub> to internally mixed inorganic and  
656 organic particles: the role of organic carbon oxidation state and inferred organic phase separations,  
657 *Atmos. Chem. Phys.*, 14, 5693-5707, <https://doi.org/10.5194/acp-14-5693-2014>, 2014.
- 658 George, C., Ponche, J., Mirabel, P., Behnke, W., Scheer, V., and Zetzsch, C.: Study of the uptake of  
659 N<sub>2</sub>O<sub>5</sub> by water and NaCl solutions, *The Journal of Physical Chemistry*, 98, 8780-8784,  
660 <https://doi.org/10.1021/j100086a031>, 1994.
- 661 Hanson, D. R., and Ravishankara, A. R.: The reaction probabilities of ClONO<sub>2</sub> and N<sub>2</sub>O<sub>5</sub> on polar  
662 stratospheric cloud materials, *Journal of Geophysical Research: Atmospheres*, 96, 5081-5090,  
663 <https://doi.org/10.1029/90jd02613>, 1991.
- 664 Hong, Y., Liu, Y., Chen, X., Fan, Q., Chen, C., Chen, X., and Wang, M.: The role of anthropogenic  
665 chlorine emission in surface ozone formation during different seasons over eastern China, *Sci. Total*  
666 *Environ.*, 723, 137697, <https://doi.org/10.1016/j.scitotenv.2020.137697>, 2020.
- 667 Huff, D. M., Joyce, P. L., Fochesatto, G. J., and Simpson, W. R.: Deposition of dinitrogen pentoxide,  
668 N<sub>2</sub>O<sub>5</sub>, to the snowpack at high latitudes, *Atmos. Chem. Phys.*, 11, 4929-4938,  
669 <https://doi.org/10.5194/acp-11-4929-2011>, 2011.
- 670 Jeong, D., McNamara, S. M., Chen, Q., Mirrielees, J., Edebeli, J., Kulju, K. D., Wang, S., Hayani, L.,  
671 Kirpes, R. M., and Lata, N. N.: Quantifying the contributions of aerosol-and snow-produced ClNO<sub>2</sub>  
672 through observations and 1D modeling, *ACS Earth Space Chem.*, 7, 2548-2561,  
673 <https://doi.org/10.1021/acsearthspacechem.3c00237>, 2023.
- 674 Kulju, K. D., McNamara, S. M., Chen, Q., Edebeli, J., Fuentes, J. D., Bertman, S. B., and Pratt, K. A.:  
675 Urban inland wintertime N<sub>2</sub>O<sub>5</sub> and ClNO<sub>2</sub> influenced by snow-covered ground, air turbulence, and  
676 precipitation, *Atmospheric Chemistry and Physics*, 2021, 1-33, [https://doi.org/10.5194/acp-22-](https://doi.org/10.5194/acp-22-2553-2022)  
677 [2553-2022](https://doi.org/10.5194/acp-22-2553-2022), 2022.
- 678 Li, Q., Zhang, L., Wang, T., Tham, Y. J., Ahmadov, R., Xue, L., Zhang, Q., and Zheng, J.: Impacts of  
679 heterogeneous uptake of dinitrogen pentoxide and chlorine activation on ozone and reactive nitrogen  
680 partitioning: improvement and application of the WRF-Chem model in southern China, *Atmos. Chem.*  
681 *Phys.*, 16, 14875-14890, <https://doi.org/10.5194/acp-16-14875-2016>, 2016.
- 682 Li, S., Liu, Y., Zhu, Y., Jin, Y., Hong, Y., Shen, A., Xu, Y., and Wang, H.: ACEIC: a comprehensive  
683 anthropogenic chlorine emission inventory for China, *Atmos. Chem. Phys.*, 24(20): p. 11521-11544,  
684 <https://doi.org/10.5194/acp-24-11521-2024>, 2024. Li, X., Zhao, W., Yang, Y., Ma, Y., Ye, J., Zhao,  
685 H., Zhang, S., Zhang, X., Xiu, A.: Impact of reactive chlorine on atmospheric oxidative capacity in a  
686 snowy polluted environment, *Environ. Sci. Technol.*, 59(36): p. 19363-19376,  
687 <https://doi.org/10.1021/acs.est.5c08841>, 2025.
- 688 Liu, Y., Fan, Q., Chen, X., Zhao, J., Ling, Z., Hong, Y., Li, W., Chen, X., Wang, M., and Wei, X.:  
689 Modeling the impact of chlorine emissions from coal combustion and prescribed waste incineration  
690 on tropospheric ozone formation in China, *Atmos. Chem. Phys.*, 18, 2709-2724,  
691 <https://doi.org/10.5194/acp-18-2709-2018>, 2018.



- 692 Lopez-Hilfiker, F. D., Constantin, K., Kercher, J. P., and Thornton, J. A.: Temperature dependent  
693 halogen activation by N<sub>2</sub>O<sub>5</sub> reactions on halide-doped ice surfaces, *Atmos. Chem. Phys.*, 12, 5237-  
694 5247, <https://doi.org/10.5194/acp-12-5237-2012>, 2012.
- 695 Lu, K. D., Rohrer, F., Holland, F., Fuchs, H., Brauers, T., Oebel, A., Dlugi, R., Hu, M., Li, X., and Lou,  
696 S. R.: Nighttime observation and chemistry of HO<sub>x</sub> in the Pearl River Delta and Beijing in summer  
697 2006, *Atmos. Chem. Phys.*, 14, 4979-4999, <https://doi.org/10.5194/acp-14-4979-2014>, 2014.
- 698 McDuffie, E. E., Fibiger, D. L., Dubé, W. P., Lopez Hilfiker, F., Lee, B. H., Jaeglé, L., Guo, H., Weber,  
699 R. J., Reeves, J. M., and Weinheimer, A. J.: ClNO<sub>2</sub> yields from aircraft measurements during the  
700 2015 WINTER campaign and critical evaluation of the current parameterization, *Journal of*  
701 *Geophysical Research: Atmospheres*, 123, 12-994, <https://doi.org/10.1029/2018jd029358>, 2018.
- 702 McDuffie, E. E., Fibiger, D. L., Dubé, W. P., Lopez Hilfiker, F., Lee, B. H., Thornton, J. A., Shah, V.,  
703 Jaeglé, L., Guo, H., and Weber, R. J.: Heterogeneous N<sub>2</sub>O<sub>5</sub> uptake during winter: Aircraft  
704 measurements during the 2015 WINTER campaign and critical evaluation of current  
705 parameterizations, *Journal of Geophysical Research: Atmospheres*, 123, 4345-4372,  
706 <https://doi.org/10.1002/2018jd028336>, 2018.
- 707 McNamara, S. M., Chen, Q., Edebeli, J., Kulju, K. D., Mumpfield, J., Fuentes, J. D., Bertman, S. B., and  
708 Pratt, K. A.: Observation of N<sub>2</sub>O<sub>5</sub> deposition and ClNO<sub>2</sub> production on the saline snowpack, *ACS*  
709 *Earth Space Chem.*, 5, 1020-1031, <https://doi.org/10.1021/acsearthspacechem.0c00317>, 2021.
- 710 McNamara, S. M., Kolesar, K. R., Wang, S., Kirpes, R. M., May, N. W., Gunsch, M. J., Cook, R. D.,  
711 Fuentes, J. D., Hornbrook, R. S., and Apel, E. C.: Observation of road salt aerosol driving inland  
712 wintertime atmospheric chlorine chemistry, *ACS Cent. Sci.*, 6, 684-694,  
713 <https://doi.org/10.1021/acscentsci.9b00994>, 2020.
- 714 McNamara, S. M., Raso, A. R., Wang, S., Thanekar, S., Boone, E. J., Kolesar, K. R., Peterson, P. K.,  
715 Simpson, W. R., Fuentes, J. D., and Shepson, P. B.: Springtime nitrogen oxide-influenced chlorine  
716 chemistry in the coastal arctic, *Environ. Sci. Technol.*, 53, 8057-8067,  
717 <https://doi.org/10.1021/acs.est.9b01797>, 2019.
- 718 Mentel, T. F., Sohn, M., and Wahner, A.: Nitrate effect in the heterogeneous hydrolysis of dinitrogen  
719 pentoxide on aqueous aerosols, *Phys. Chem. Chem. Phys.*, 1, 5451-5457,  
720 <https://doi.org/10.1039/a905338g>, 1999.
- 721 Mielke, L. H., Stutz, J., Tsai, C., Hurlock, S. C., Roberts, J. M., Veres, P. R., Froyd, K. D., Hayes, P. L.,  
722 Cubison, M. J., and Jimenez, J. L.: Heterogeneous formation of nitryl chloride and its role as a  
723 nocturnal NO<sub>x</sub> reservoir species during CalNex-LA 2010, *Journal of Geophysical Research:*  
724 *Atmospheres*, 118, 10-638, <https://doi.org/10.1002/jgrd.50783>, 2013.
- 725 Tham, Y. J., Wang, Z., Li, Q., Wang, W., Wang, X., Lu, K., Ma, N., Yan, C., Kecorius, S., and  
726 Wiedensohler, A.: Heterogeneous N<sub>2</sub>O<sub>5</sub> uptake coefficient and production yield of ClNO<sub>2</sub> in  
727 polluted northern China: roles of aerosol water content and chemical composition, *Atmos. Chem.*  
728 *Phys.*, 18, 13155-13171, <https://doi.org/10.5194/acp-18-13155-2018>, 2018.
- 729 Thornton, J. A., and Abbatt, J. P.: N<sub>2</sub>O<sub>5</sub> reaction on submicron sea salt aerosol: Kinetics, products, and  
730 the effect of surface active organics, *The Journal of Physical Chemistry A*, 109, 10004-10012,  
731 <https://doi.org/10.1021/jp054183t>, 2005.
- 732 Wagner, N. L., Riedel, T. P., Young, C. J., Bahreini, R., Brock, C. A., Dubé, W. P., Kim, S., Middlebrook,  
733 A. M., Öztürk, F., and Roberts, J. M.: N<sub>2</sub>O<sub>5</sub> uptake coefficients and nocturnal NO<sub>2</sub> removal rates  
734 determined from ambient wintertime measurements, *Journal of Geophysical Research: Atmospheres*,  
735 118, 9331-9350, <https://doi.org/10.1002/jgrd.50653>, 2013.



- 736 Wang, S., McNamara, S. M., Kolesar, K. R., May, N. W., Fuentes, J. D., Cook, R. D., Gansch, M. J.,  
737 Mattson, C. N., Hornbrook, R. S., and Apel, E. C.: Urban snowpack ClNO<sub>2</sub> production and fate: A  
738 one-dimensional modeling Study, *ACS Earth Space Chem.*, 4, 1140-1148,  
739 <https://doi.org/10.1021/acsearthspacechem.0c00116>, 2020.
- 740 Wang, X., Jacob, D. J., Eastham, S. D., Sulprizio, M. P., Zhu, L., Chen, Q., Alexander, B., Sherwen, T.,  
741 Evans, M. J., and Lee, B. H.: The role of chlorine in global tropospheric chemistry, *Atmos. Chem.*  
742 *Phys.*, 19, 3981-4003, <https://doi.org/10.5194/acp-19-3981-2019>, 2019.
- 743 Wang, X., Jacob, D. J., Fu, X., Wang, T., Breton, M. L., Hallquist, M., Liu, Z., McDuffie, E. E., and  
744 Liao, H.: Effects of anthropogenic chlorine on PM<sub>2.5</sub> and ozone air quality in China, *Environ. Sci.*  
745 *Technol.*, 54, 9908-9916, <https://doi.org/10.1021/acs.est.0c02296>, 2020.
- 746 Wang, X., Wang, H., Xue, L., Wang, T., Wang, L., Gu, R., Wang, W., Tham, Y. J., and Wang, Z.:  
747 Observations of N<sub>2</sub>O<sub>5</sub> and ClNO<sub>2</sub> at a polluted urban surface site in North China: High N<sub>2</sub>O<sub>5</sub> uptake  
748 coefficients and low ClNO<sub>2</sub> product yields, *Atmos Environ*, 156, p. 125-134,  
749 <https://dx.doi.org/10.1016/j.atmosenv.2017.02.035>, 2017.
- 750 Xia, M., Peng, X., Wang, W., Yu, C., Sun, P., Li, Y., Liu, Y., Xu, Z., Wang, Z., and Xu, Z.: Significant  
751 production of ClNO<sub>2</sub> and possible source of Cl<sub>2</sub> from N<sub>2</sub>O<sub>5</sub> uptake at a suburban site in eastern China,  
752 *Atmos. Chem. Phys.*, 20, 6147-6158, <https://doi.org/10.5194/egusphere-egu2020-12946>, 2020.
- 753 Xia, M., Peng, X., Wang, W., Yu, C., Wang, Z., Tham, Y. J., Chen, J., Chen, H., Mu, Y., and Zhang, C.:  
754 Winter ClNO<sub>2</sub> formation in the region of fresh anthropogenic emissions: seasonal variability and  
755 insights into daytime peaks in northern China, *Atmos. Chem. Phys.*, 21, 15985-16000,  
756 <https://doi.org/10.5194/acp-21-15985-2021>, 2021.
- 757 Xie, S., Qi, H., Xiu, A., Zhang, X., Lu, L., Jiang, J., Liu, Y., and Liu, S.: The impact of anthropogenic  
758 chlorine emissions from coal combustion during the winter snow period on atmospheric ClNO<sub>2</sub>,  
759 *Environ. Chem.*, 44, 1356-1369, DOI:10.7524/j.issn.0254-6108.2024081101, 2025.
- 760 Yang, X., Wang, Q., Ma, N., Hu, W., Gao, Y., Huang, Z., Zheng, J., Yuan, B., Yang, N., and Tao, J.:  
761 The impact of chlorine chemistry combined with heterogeneous N<sub>2</sub>O<sub>5</sub> reactions on air quality in  
762 China, *Atmos. Chem. Phys.*, 22, 3743-3762, <https://doi.org/10.5194/acp-22-3743-2022>, 2022.
- 763 Yi, X., Yin, S., Huang, L., Li, H., Wang, Y., Wang, Q., Chan, A., Traoré, D., Ooi, M. C. G., and Chen,  
764 Y.: Anthropogenic emissions of atomic chlorine precursors in the Yangtze River Delta region, China,  
765 *Sci. Total Environ.*, 771, 144644, <https://doi.org/10.1016/j.scitotenv.2020.144644>, 2021.
- 766 Yu, C., Wang, Z., Xia, M., Fu, X., Wang, W., Tham, Y. J., Chen, T., Zheng, P., Li, H., and Shan, Y.:  
767 Heterogeneous N<sub>2</sub>O<sub>5</sub> reactions on atmospheric aerosols at four Chinese sites: Improving model  
768 representation of uptake parameters, *Atmos. Chem. Phys.*, 20, 4367-4378,  
769 <https://doi.org/10.5194/acp-20-4367-2020>, 2020.
- 770 Zhu, Q., Laughner, J. L., and Cohen, R. C.: Combining machine learning and satellite observations to  
771 predict spatial and temporal variation of near surface OH in North American cities, *Environ. Sci.*  
772 *Technol.*, 56, 7362-7371, <https://doi.org/10.1021/acs.est.1c05636>, 2022.